Available online at www.sciencedirect.com
ScienceDirect
Trans. Nonferrous Met. Soc. China 26(2016) 2051−2057
Transactions of Nonferrous Metals Society of China
www.tnmsc.cn

Influence of Sn addition on mechanical properties of gas tungsten arc welded AM60 Mg alloy sheets

Jun GOU[1,2], Ai-tao TANG[1,2], Fu-sheng PAN[1,2,3], Jia SHE[1,4,5], Su-qin LUO[1,3], Jun-hua YE[1,2], Da-wei SHI[1,2], M. RASHAD[1,2]

1. College of Materials Science and Engineering, Chongqing University, Chongqing 400044, China;
2. National Engineering Research Center for Magnesium Alloys, Chongqing University, Chongqing 400044, China;
3. Chongqing Academy of Science and Technology, Chongqing 401123, China;
4. Science and Technology on Reactor System Design Technology Laboratory, Nuclear Power Institute of China, Chengdu 610041, China;
5. College of Materials Science and Engineering, Guilin University of Technology, Guilin 541004, China

Received 29 August 2015; accepted 11 April 2016

Abstract: The effects of Sn addition on the microstructure and mechanical properties of gas tungsten arc butt-welded Mg−6Al−0.3Mn (AM60) (mass fraction, %) alloy sheets were investigated by optical microscopy, scanning electron microscopy, X-ray diffraction, transmission electron microscopy, and microhardness and tensile tests. The results indicate that both the average microhardness and joint efficiency of AM60 are improved by the addition of 1% Sn (mass fraction). The ultimate tensile strength of Mg−6Al−1Sn−0.3Mn (ATM610) reaches up to 96.8% of that of base material. Moreover, fracture occurs in the fusion zone of ATM610 instead of in the heat-affected zone of AM60 welded joint. The improvement in the properties is mainly attributed to the formation of Mg_2Sn, which effectively obstructs the grain coarsening in the heat-affected zone, resulting in a relatively fine microstructure. The addition of 1% Sn improves the mechanical properties of AM60 welded joint.

Key words: AM60 Mg alloy; ATM610 Mg alloy; gas tungsten arc welding; mechanical properties

1 Introduction

Magnesium is one of the most abundant elements in the earth's surface. Mg-based materials are considered environmentally friendly engineering materials with great prospect in the 21 century considering the demands for energy saving and environment protection [1,2]. Mg alloys have attracted considerable attention from automotive and aerospace industries, wherein weight saving is important owing to their light weight, low density, high specific strength, and good damping capacity [3]. Moreover, Mg alloys have good casting property, dimensional accuracy, electromagnetic compatibility interference shielding, and excellent machinability, which may promote further utilization [4]. Nonetheless, a reliable joining process is necessary for the wide application of Mg alloys. Currently, many welding methods are available, and gas tungsten arc welding (GTAW) based on tungsten alloy electrode, with argon as shielding gas in most cases, is extensively used to weld Mg alloys on account of its advantages in terms of utility and economy [1].

The AM60 Mg alloy series are characterized by reduced weight, which is attractive for the manufacture of electronic devices, sport equipments, hand tools, automobiles, and aerospace gear [5,6]. The previous reports indicated that Sn addition could improve the microstructure and mechanical properties of Mg−Al-based alloys [7,8]. WEI et al [9] attributed the improvement of the mechanical properties in Sn-containing alloys to the increase of volume fraction of secondary phases and the modification in the shaping process of eutectic $Mg_{17}Al_{12}$. SASAKI et al [10]

Foundation item: Project (51474043) supported by the National Natural Science Foundation of China; Project (2014DFG52810) supported by the Ministry of Science and Technology of China; Projects (SRFDR 20130191110018, CDJZR13130086) supported by the Ministry of Education of China; Project (CSTC2013JCYJC60001) supported by the Chongqing Municipal Government, China; Projects (CSTC2012ggB50003, CSTC2013jjB50006) supported by the Natural Science Foundation of Chongqing Science and Technology Commission, China
Corresponding author: Ai-tao TANG; Tel: +86-23-65106121; E-mail: tat@cqu.edu.cn
DOI: 10.1016/S1003-6326(16)64298-X

contributed the strength improvement to the formation of dispersed short rod-like Mg_2Sn particles, resulting from a minor addition of Sn. XIANG et al [11] also found that the addition of Sn can improve the strength of the alloys by the development of Mg_2Sn phase and refining effect. Similarly, YANG and PAN [12] indicated that the improvement is possibly ascribed to the effects of Sn addition on the morphology and size of $Mg_{32}(Al, Zn)_{49}$ phases at the grain boundaries. Fine and uniform phases distributed along grain boundaries act as effective hindrance to impede dislocation motion, thus improving the properties of engineering alloys.

Thus, the addition of Sn can improve the properties of Mg alloys. Determining whether Sn addition is helpful for the welding of Mg alloys is indispensable in the manufacturing industry. This investigation aimed to explore the weldability of AM60 Mg alloy sheets with Sn addition.

2 Experimental

ATM610 and AM60 Mg alloys were fabricated in a low-carbon steel crucible resistance furnace protected by a gas mixture (CO_2 + SF_6). Melting was operated at 1013 K for 10 min. The refining agent was then added, and the mixture was homogenized by mechanical stirring at 300 r/min. After complete mixing, the melt was held at 1013 K for 20 min. After cooling to 993 K, the melt was poured into a permanent metal mold (a specific Fe alloy die with a dead head to obtain a perfect cylindrical cast), and then preheated to around 573 K for casting.

The synthesized alloys were homogenized at 703 K for 24 h, followed by water-quenching to induce a supersaturated solid solution. The ingots were preheated at 623 K for 1 h and extruded at 623 K by applying a controlled and constant force using an XJ–500 horizontal extrusion machine. The extrusion ratio was 25:1 and the ram speed was set at 1 m/min.

The extruded sheets (3 mm in thickness) of AM60 and ATM610 Mg alloys were cut into the required size (120 mm × 60 mm) by machining process. The nominal compositions of base materials and AM60 filler metal are listed in Table 1. Square-butted joint configuration was adopted, and the samples were welded by automatic GTAW equipment with Panasonic YC−300WX power source, where AM60 was used as the filler metal. An overall view of the welding equipment is shown in Fig. 1. Optimal welding parameters were determined (Table 2), and all samples were under the same condition.

Prior to welding, the surfaces of samples and wires were cleaned by sanding, washed with water and ethanol, and then dried. Further grooving was unnecessary for the reason of thickness. After welding procedure, to avoid the influence of welding drawbacks, only the parts of the joints which were free of defects were machined into tensile specimens in the form of a gauge section (24 mm in length and 6 mm in width), according to ASTM E8M sheet type material standard (Fig. 2). Three standard tensile specimens with the humping bead eliminated were sectioned from each welded joint sample containing the weld in the center of the gauge length. The ultimate tensile strength (UTS) data represent average values acquired on a hydraulic tensile machine at a cross-head velocity of 0.6 mm/min. Microhardness was measured on the cross-section perpendicular to the welding direction using a Vickers hardness digital tester (MH−6) at a dwell period of 5 s, a load of 1 N, and a step size of 0.5 mm.

The specimens for metallographic examination were sliced to appropriate size and polished using different grades of emery papers, and then etched in a saturated

Table 1 Nominal compositions of base materials and AM60 filler metal (mass fraction, %)

Sample	Al	Mn	Sn	Mg
AM60	6.0	0.3	0	Bal.
ATM610	6.0	0.3	1	Bal.

Table 2 Parameters of GTAW

Designation	Value
Tungsten diameter/mm	2.4
Filler wire diameter/mm	2.5
Welding current/A	105
Welding speed/(mm·s^{-1})	3.1
Wire feed rate/(mm·s^{-1})	11
Gas flow rate/min^{-1}	10

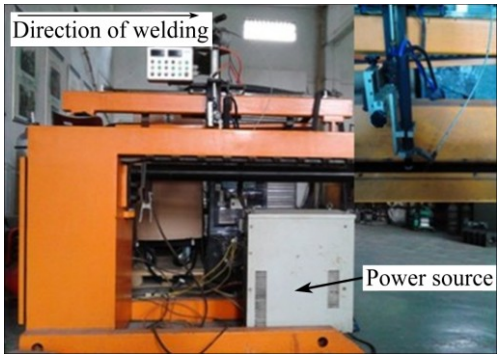

Fig. 1 Equipment utilized in GTAW (Inset showing location of wire feeder in relation to tungsten electrode)

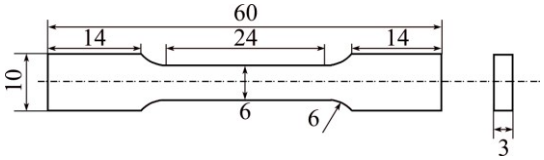

Fig. 2 Dimensions of specimen used for tensile test (unit: mm)

solution of ethanol, acetic acid, and picric acid (the volume ratio of ethanol to acetic acid is 8:1) for about 20 s until the microstructures were conspicuously revealed. The microstructure was observed by optical microscopy (OM) and scanning electron microscopy (SEM). The distribution of alloying elements was evaluated by energy-dispersive X-ray spectroscopy (EDS). The grain diameter was collected in three separate directions in each grain (ASTM E 112–88) from at least five separate OM images using Image-Pro Plus software. The secondary phases in the as-extruded alloys were characterized by transmission electron microscopy (TEM, ZEISS Libra 200 FE) using an accelerating voltage of 200 kV. In addition, X-ray diffraction (XRD) was employed to identify the phases in the weld. Finally, fracture appearance was evaluated by SEM.

3 Results

3.1 Macrograph of welded joint

Welded joints with similar appearance irrespective of which alloys they are obtained by optimizing the process parameters. The macro-morphologies of the welding seam are shown Fig. 3, where typical welding scale can be seen in one side and, at the same time, over-penetration happens on the other side.

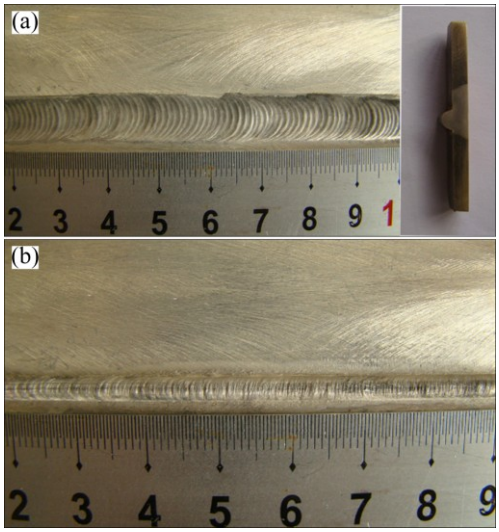

Fig. 3 Macro-morphologies of welded seam: (a) Front face; (b) Back face

3.2 Microstructures

As shown in Fig. 4, the microstructures of base materials consist of equiaxed grains, which are attributed to dynamic recrystallization (DRX) during hot extrusion. The average grain sizes of basal materials of AM60 and ATM610 are ~31 and ~40 μm, respectively. Thus, DRX is promoted by the addition of Sn. The welded joints are typically composed of fusion zone (FZ), heat-affected zone (HAZ), and base material (BM), as shown in Fig. 5. The microstructure in FZ presents finer equiaxed grains with intergranular $Mg_{17}Al_{12}$ precipitates (β phase), because rapid cooling induced by good thermal conductivity and low thermal capacity of Mg hampers

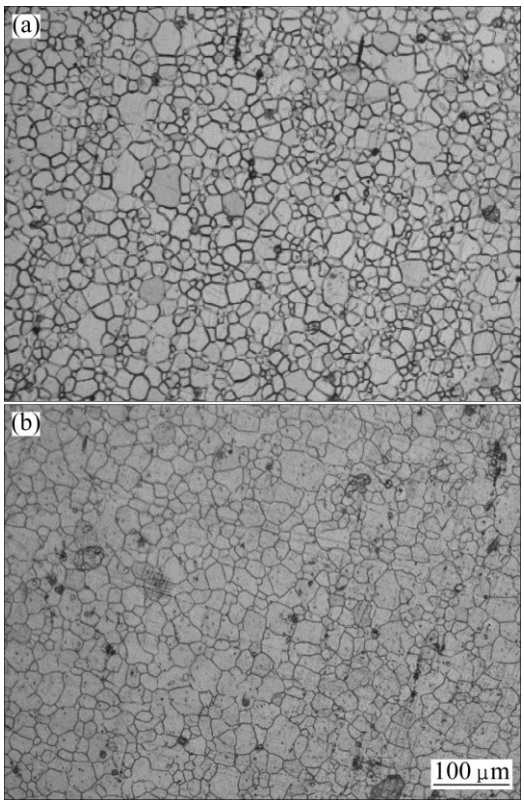

Fig. 4 Microstructures of base materials of AM60 (a) and ATM610 (b)

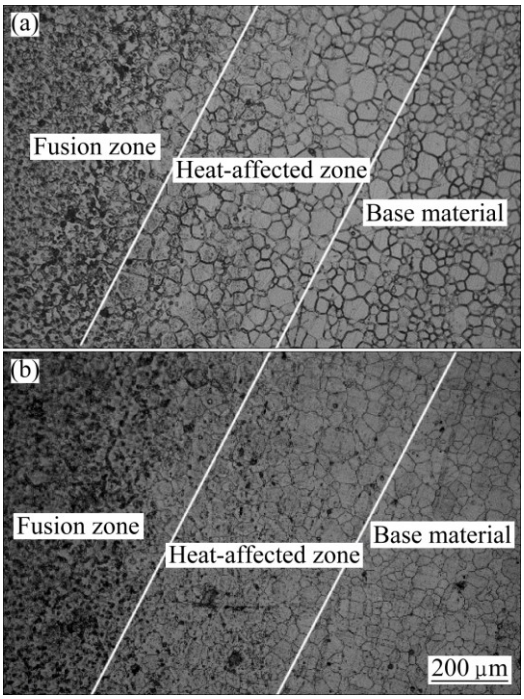

Fig. 5 Microstructures of welded joints: (a) GTAWed AM60; (b) GTAWed ATM610

the growth of grains in FZ [13]. However, the grains in HAZ undergo a degree of overheat absorbed from FZ, offering enough driving force to form coarse grains. During the welding process, the temperature in HAZ may be up to 527 K [14−16], which exceeds the recrystallization temperature of the Mg−Al alloys series (~478 K [17]). Moreover, the stored energy caused by extrusion is relatively high, resulting in unstable grains [18]. Therefore, recrystallization and grain coarsening can easily occur in HAZ. More importantly, Fig. 5 shows that the grains in HAZ of ATM610 are only slightly larger than those in BM, in contrast to the HAZ of AM60 where the grain size is remarkably coarser than that of BM. The average grain sizes in HAZ of AM60 and ATM610 are ~43.4 and ~46 μm, respectively.

XRD was employed to identify the primary phases in FZ (Fig. 6). Determining a second phase containing Sn or Mn is difficult because of too low amounts of Sn and Mn. Conversely, Al accounts for large fraction in the alloys, as such, only α-Mg and $Mg_{17}Al_{12}$ were detected. In addition, according to the Mg−Sn binary phase diagram, Sn may be dissolved into the Mg matrix at low Sn content, and only a little Mg_2Sn was produced. Moreover, the presence of 1% Sn and 0.3% Mn in ATM60 does not change the major phases in the base material and the weld.

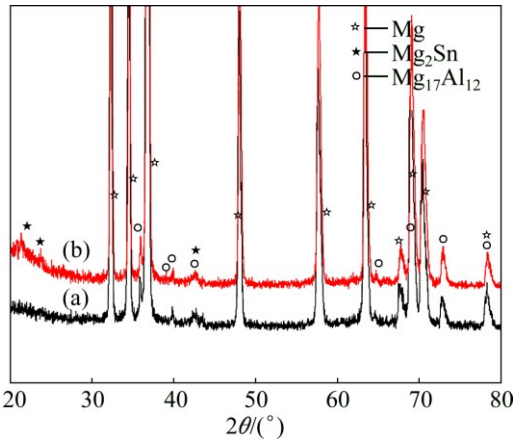

Fig. 6 XRD patterns of AM60 (a) and ATM610 (b) sheets

The comparison of the SEM images of FZ of AM60 and ATM610 alloys shows that the $Mg_{17}Al_{12}$ phase of ATM610 alloy is much larger than that of AM60 alloy (Fig. 7). In addition, the backscattered SEM image of ATM610 alloy (inset of Fig. 7(b)) shows that finer Mg_2Sn intermetallics (bright spots) are embedded into the $Mg_{17}Al_{12}$ phase (gray convex phase) in the ATM610 alloy.

3.3 Mechanical properties

Figure 8 shows the Vickers microhardness profiles of AM60 and ATM610 measured along the mid-thickness

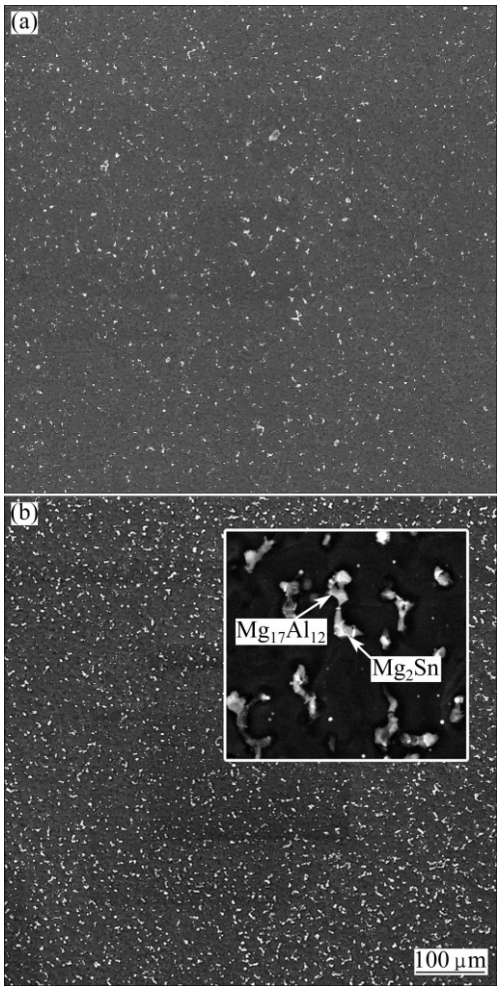

Fig. 7 SEM images of fusion zones of welded joints: (a) AM60; (b) ATM610

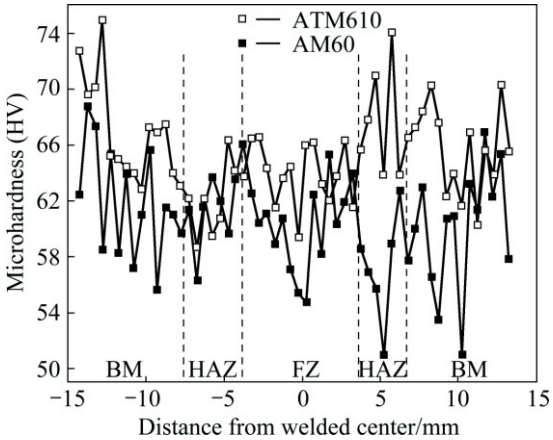

Fig. 8 Microhardness variations of ATM610 and AM60 as function of distance

line of the cross-section, in which 0 means the center of weld seam. The average hardness of ATM610 (HV 65.3) is generally higher than that of AM60 (HV 60.5) across the whole transverse section. In particular, the hardness values of BM of the two alloys differ in varying points,

which is mainly ascribed to various grain sizes and gain boundary with diverse microstructures, even second-phase particles appear sparsely. When the HAZ of AM60 on the right side presents low hardness value, the hardness of HAZ of ATM610 remains constant as high as that of BM, or even higher. This finding is attributed to similar grain size with that of BM, as well as the excellent solution hardening with Sn addition.

The welded specimens used for tensile test were cut by linear intercept method, and the humping bead was eliminated before the test. Considering the effect of fabrication, all specimens should be leveled and cleaned, as illustrated in Fig. 9. The test results obtained at ambient temperature are illustrated in Fig. 10. After welding, the UTS (σ_b) and elongation (δ) of welded joints decrease noticeably. As shown in Table 3, the UTS and elongation of initial alloys are approximately the same. After welding, the UTS of AM60 decreases by 19.5 MPa, whereas the value for ATM610 decreases merely by 8.9 MPa. Thus, the joint efficiencies of AM60 and ATM610 are 92.9% and 96.8%, respectively. Similarly, when the reduction of elongation of AM60 is 11.3%, the corresponding value for ATM610 is 8.9%. Therefore, ATM610 exhibits considerably better weldability than AM60 under identical process parameters.

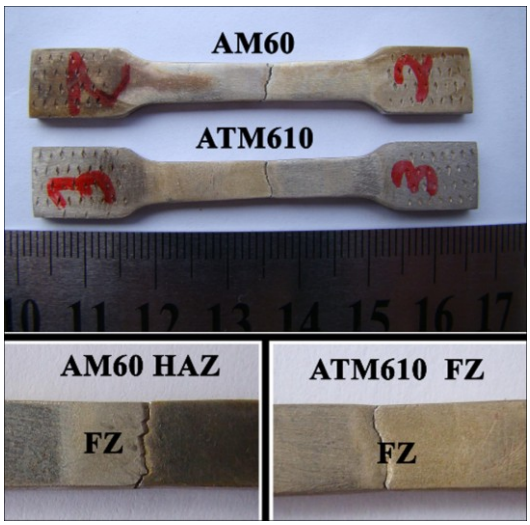

Fig. 9 Tensile specimens and fracture locations

Table 3 Mechanical properties of base material and welded joint

Sample	σ_b/MPa	δ/%
AM60	274.6±3.1	27.2±1.1
wAM60	255.1±4.0	15.9±2.4
ATM610	274.3±2.7	25.9±1.5
wATM610	265.4±3.8	17.0±2.2

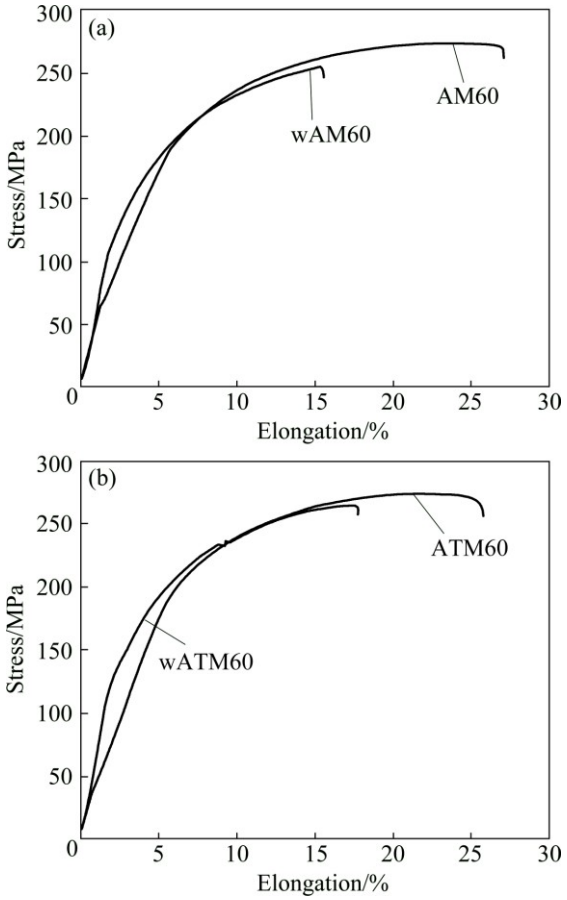

Fig. 10 Stress–strain curves of AM60 (a) and ATM610 (b) before and after welding

4 Discussion

SHE et al [7] reported that during the solidification of Mg−Al−Sn-based alloys, α-Mg phase first nucleates and then grows. With the decrease of temperature, Mg_2Sn intermetallic nuclei form, which then act as heterogeneous nucleation sites of $Mg_{17}Al_{12}$; subsequently, the $Mg_{17}Al_{12}$ is generated on the habit plane of Mg_2Sn from the eutectic reaction $L\rightarrow\alpha$-Mg+$Mg_{17}Al_{12}$+Mg_2Sn [19]. The orientation relationship between $Mg_{17}Al_{12}$ and Mg_2Sn is $(220)_{Mg_2Sn}$ 1.11° from $(330)_{Mg_{17}Al_{12}}$, $\langle 001\rangle_{Mg_2Sn}$// $\langle 22\bar{1}\rangle_{Mg_{17}Al_{12}}$ [7]. Therefore, the $Mg_{17}Al_{12}$ phase in the FZ of ATM610 alloy is larger than that of AM60 alloy.

Figure 11 shows the bright-field TEM image of ATM610. Fine Mg_2Sn and $Mg_{17}Al_{12}$ precipitates distribute uniformly in the Mg matrix and the coarse particles (indicated by arrows) are Mg_2Sn precipitates. JUNG et al [20] found that fine $Mg_{17}Al_{12}$ precipitates generated by aging prior to extrusion effectively reduce the average size of DRXed grains in Mg−7.6Al−0.4Zn extruded alloy. PAN et al [21] also indicated that the formation of fine DRXed grains in extruded Mg−Ca alloy is attributed to the effective pinning of DRXed

grain boundaries by pre-formed precipitates. DENG et al [22] reported that secondary $Al_3Sc_xZr_{(1-x)}$ particles originally presented in parent alloy become coarse during the TIG welding process; these particles can restrain the grain growth and effectively improve the welding performance. The dominant reason for the improved UTS is that fine secondary Mg_2Sn particles form in the AM60 Mg matrix with proper Sn addition. Mg_2Sn is a hard phase with high melting point (~1043 K) that can effectively hinder grain coarsening during welding. The grain growth in the HAZ of AM60 is more obvious than that of ATM610. Thus, ATM610 possesses considerably better weldability than AM60.

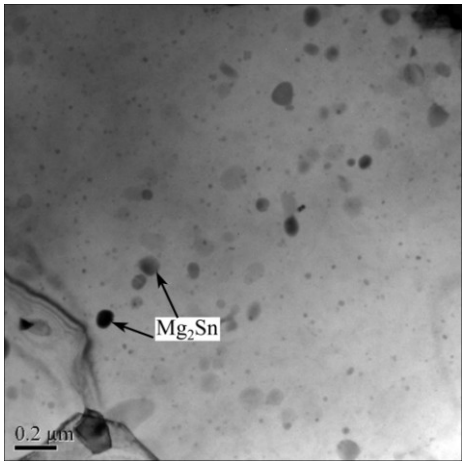

Fig. 11 Bright-field TEM image of ATM610

The tensile properties of the welded Mg alloys depend on several microstructural factors, such as grain size, dislocation density, and crystallographic orientation [23]. The fractures of AM60 occur in the HAZ because of the presence of coarse grains, thereby reducing the strength according to the Hall−Petch equation, which indicates that the change of strength is inversely proportional to the square root of grain size. On the contrary, the fractures of ATM610 specimens occur in the FZ. A number of second-phase particles (β-$Mg_{17}Al_{12}$), as shown in Fig 7, precipitate along the grain boundary producing local stress concentration [24], and β phase is a hard phase that promotes the formation of crack. Hence, the cracks may initiate at the brittle β phase along the grain boundaries [25]. More importantly, the HAZ of ATM610 is no longer a weak area because its grain size is almost equivalent to that of BM. For ATM610, the fracture location changes from the HAZ to FZ, as shown in Fig. 9.

5 Conclusions

1) The joint efficiency is improved from 92.9% to 96.8% by adding 1% Sn to AM60 using the same optimal process parameters.

2) The decrease of ductility of ATM610 joint is lesser than that of AM60 joint after welding. The reductions of elongation of AM60 and ATM610 are 11.3% and 8.9%, respectively.

3) The microhardness in all zones of ATM610 is generally higher than that of AM60 across the whole transverse welded joint because of Sn-induced solution hardening.

References

[1] LIU L M. Welding and joining of magnesium alloys [M]. Cambridge: Woodhead Publishing, 2010.

[2] LUO A A. Magnesium casting technology for structural applications [J]. Journal of Magnesium and Alloys, 2013, 1(1): 2−22.

[3] GUO L, FUJITA F. Influence of rolling parameters on dynamically recrystallized microstructures in AZ31 magnesium alloy sheets [J]. Journal of Magnesium and Alloys, 2015, 3(2): 95−105.

[4] LIU X, HAO H, ZHU X, ZHANG X. Grain refining effect of Mg by novel particle cluster-containing Al−Ti−C master alloy [J]. Transactions of Nonferrous Metals Society of China, 2015, 25(6): 1804−1810.

[5] KULYASOVA O, ISLAMGALIEV R, MINGLER B, ZEHETBAUER M. Microstructure and fatigue properties of the ultrafine-grained AM60 magnesium alloy processed by equal-channel angular pressing [J]. Materials Science and Engineering A, 2009, 503(1−2): 176−180.

[6] SEVIK H, AÇIKGÖZ S, CAN K S. The effect of tin addition on the microstructure and mechanical properties of squeeze cast AM60 alloy [J]. Journal of Alloys and Compounds, 2010, 508(1): 110−114.

[7] SHE J, PAN F, HU H, TANG A, YU Z, SONG K. Effect of Mg_2Sn intermetallic on the grain refinement in as-cast AM series alloy [J]. Journal of Materials Engineering and Performance, 2015, 24(8): 2937−2943.

[8] SHE J, PAN F, PENG P, TANG A, YU Z, WU L, PAN H, ZHAO C, GAO Z, LUO S, RASHAD M. Microstructure and mechanical properties of asextruded Mg−xAl−5Sn−0.3Mn alloys (x=1, 3, 6 and 9) [J]. Materials Science and Technology, 2015, 31(3): 344−348.

[9] WEI S, ZHU T, HODGSON M, GAO W. Effects of Sn addition on the microstructure and mechanical properties of as-cast, rolled and annealed Mg−4Zn alloys [J]. Materials Science and Engineering A, 2013, 585(15): 139−148.

[10] SASAKI T T, YAMAMOTO K, HONMA T, KAMADO S, HONO K. A high-strength Mg−Sn−Zn−Al alloy extruded at low temperature [J]. Scripta Materialia, 2008, 59(10): 1111−1114.

[11] XIANG Q, WU R, ZHANG M. Influence of Sn on microstructure and mechanical properties of Mg−5Li−3Al−2Zn alloys [J]. Journal of Alloys and Compounds, 2009, 477(1−2): 832−835.

[12] YANG M, PAN F. Effects of Sn addition on as-cast microstructure, mechanical properties and casting fluidity of ZA84 magnesium alloy [J]. Materials and Design, 2010, 31(1): 68−75.

[13] LIU L, DONG C. Gas tungsten-arc filler welding of AZ31 magnesium alloy [J]. Materials Letters, 2006, 60(17−18): 2194−2197.

[14] LIANG G, YUAN S. Study on the temperature measurement of AZ31B magnesium alloy in gas tungsten arc welding [J]. Materials Letters, 2008, 62(15): 2282−2284.

[15] WEN Tong, LIU Shi-yao, CHEN Shi, LIU Lan-tao, YANG Chen. Influence of high frequency vibration on microstructure and mechanical properties of TIG welding joints of AZ31 magnesium alloy [J]. Transactions of Nonferrous Metals Society of China, 2015, 25(2): 397−404.

[16] SUBRAVEL V, PADMANABAN G, BALASUBRAMANIAN V. Effect of welding speed on microstructural characteristics and tensile properties of GTA welded AZ31B magnesium alloy [J]. Transactions of Nonferrous Metals Society of China, 2014, 24(9): 2776−2784.
[17] SAKAI T, BELYAKOV A, KAIBYSHEV R, MIURA H, JONAS J J. Dynamic and post-dynamic recrystallization under hot, cold and severe plastic deformation conditions [J]. Progress in Materials Science, 2014, 60: 130−207.
[18] LIU X, GU S, WU R, LENG X, YAN J, ZHANG M. Microstructure and mechanical properties of Mg−Li alloy after TIG welding [J]. Transactions of Nonferrous Metals Society of China, 2011, 21(3): 477−481.
[19] DOERNBERG E, KOZLOV A, SCHMID-FETZER R. Experimental investigation and thermodynamic calculation of Mg−Al−Sn phase equilibria and solidification microstructures [J]. Journal of Phase Equilibria and Diffusion, 2007, 28(6): 523−535.
[20] JUNG J, PARK S H, YU H, KIM Y M, LEE Y K, YOU B S. Improved mechanical properties of Mg−7.6Al−0.4Zn alloy through aging prior to extrusion [J]. Scripta Materialia, 2014, 93(15): 8−11.
[21] PAN H, QIN G, REN Y, WANG L, SUN S, MENG X. Achieving high strength in indirectly-extruded binary Mg−Ca alloy containing Guinier–Preston zones [J]. Journal of Alloys and Compounds, 2015, 630(5): 272−276.
[22] DENG Y, PENG B, XU G, PAN Q, YIN Z, YE R, WANG Y, LU L. Effects of Sc and Zr on mechanical property and microstructure of tungsten inert gas and friction stir welded aerospace high strength Al−Zn−Mg alloys [J]. Materials Science and Engineering A, 2015, 639(15): 500−513.
[23] PARK S H C, SATO Y S, KOKAWA H. Effect of micro-texture on fracture location in friction stir weld of Mg alloy AZ61 during tensile test [J]. Scripta Materialia, 2003, 49(2): 161−166.
[24] ZHANG Z, LIU L, SHEN Y, WANG L. Mechanical properties and microstructures of a magnesium alloy gas tungsten arc welded with a cadmium chloride flux [J]. Materials Characterization, 2008, 59(1): 40−46.
[25] MIN D, SHEN J, LAI S, CHEN J. Effect of heat input on the microstructure and mechanical properties of tungsten inert gas arc butt-welded AZ61 magnesium alloy plates [J]. Materials Characterization, 2009, 60(12): 1583−1590.

添加 Sn 对钨极氩弧焊接 AM60 镁合金板材力学性能的影响

苟 军[1,2]，汤爱涛[1,2]，潘复生[1,2,3]，佘 加[1,4,5]，罗素琴[1,3]，叶俊华[1,2]，石大伟[1,2]，M. RASHAD[1,2]

1. 重庆大学 材料科学与工程学院，重庆 400044；
2. 重庆大学 国家镁合金材料工程技术研究中心，重庆 400044；
3. 重庆科学技术研究院，重庆 401123；
4. 中国核动力研究设计院 核反应堆系统设计技术重点实验室，成都 610041；
5. 桂林理工大学 材料科学与工程学院，桂林 541004

摘 要：利用光学显微镜、扫描电镜、透射电镜、X 射线衍射、硬度和拉伸实验研究 Sn 添加对钨极氩弧焊接 Mg−6Al−0.3Mn(质量分数，%)(AM60)合金板材的显微组织和力学性能的影响。结果表明：向 AM60 镁合金中添加 1%(质量分数)的 Sn 后，即 Mg−6Al−1Sn−0.3Mn (ATM610)，其焊缝的硬度和接头效率均提高。ATM610 镁合金焊缝抗拉强度达到母材的 96.8%，且断裂位置也由热影响区转移至熔合区。焊接性能的改善主要源于合金中 Mg_2Sn 有效阻碍热影响区晶粒的长大而形成的细小显微组织。在 AM60 镁合金中添加 1%的 Sn 可改善其力学性能。

关键词：AM60 镁合金；ATM610 镁合金；Sn 添加；钨极氩弧焊接；力学性能

(Edited by Mu-lan QIN)